Granular coarsening: Phase space and evolution analogies

Gabriel Juarez,[1] Richard M. Lueptow,[2] and Julio M. Ottino[2,3,4,*]
[1]*Department of Physics and Astronomy, Northwestern University, Evanston, Illinois 60208, USA*
[2]*Department of Mechanical Engineering, Northwestern University, Evanston, Illinois 60208, USA*
[3]*Department of Chemical and Biological Engineering, Northwestern University, Evanston, Illinois 60208, USA*
[4]*The Northwestern Institute on Complex Systems (NICO), Northwestern University, Evanston, Illinois 60208, USA*
(Received 19 March 2009; revised manuscript received 5 December 2009; published 8 January 2010)

Various aspects of axial banding of size-varying bidisperse granular mixtures in cylindrical tumblers have been documented repeatedly over a decade or so, but the dependence of surface band formation on the relative concentration of particles and rotation rate has not been thoroughly examined. Coarsening patterns analogous to nucleation and spinodal decomposition occur as the relative concentration of small and large particles and the rotation rate of the tumbler are varied. A phase diagram with a portion analogous to a miscibility gap can be constructed from the space-time plots. A dynamic scaling approach similar to that for reacting lamellae can be applied to the coarsening patterns as a result of large bands growing at the expense of neighboring smaller bands.

DOI: 10.1103/PhysRevE.81.012301 PACS number(s): 45.70.−n, 64.75.−g, 89.75.Da

I. INTRODUCTION

Bidisperse mixtures of particles of different sizes segregate into alternating surface bands of individual components (with a core of small particles below the surface) along the axis of a rotating tumbler instead of remaining well mixed [1–4]. Although numerous experiments have investigated the effects of particle size [3,5,6], fill level [4,6,7], particle restitution coefficient [6,7], tumbler geometry [5,8–10], rotational speed [4–7,9,11–14], and interstitial fluid [9,12,13,15], a theoretical framework that can describe and predict mixing and segregation remains an open problem.

Axial banding has been compared to spinodal decomposition [2,3,16]. However, the analogy has not been explored in the context of the *entire* phase diagram or with respect to nucleation. Our recent work on how the mixture composition affects the evolution of axial segregation [17] provides a starting point for such exploration. In fact, the large amount of information available provides the motivation to seek alternative approaches to make sense of the data. This paper proposes two analogies for axial segregation patterns of a size-varying granular mixture. The first points to similarities between the phase diagram of a prototypical chemical binary mixture and the phase diagram of space-time plots for the granular system. The second uses a scaling approach previously used to describe the dynamics of lamellae produced by chaotic mixing of fluids [18,19]. While the physics of these systems is clearly different, the analogies are useful to qualitatively understand the data.

II. EXPERIMENTAL METHODS

Data were obtained using a method identical to that used in our previous work [17]. Briefly, a horizontal acrylic tube of length $L=75$ cm and inner diameter $D=6.35$ cm was partially filled with a mixture of $d_S=0.6$ mm (0.57 ± 0.08 mm) smooth, spherical silver glass beads ($\rho=2.4$ g/cm^3) and $d_L=2$ mm (2.0 ± 0.06 mm) smooth, spherical black basalt beads ($\rho=2.6$ g/cm^3). The mixture was completely submerged in tap water. The volume concentrations of small particles, c_s, varied as 10%, 20%, 30%, 40%, 50%, 60%, 70%, 80%, and 90%. A graduated cylinder was used to measure the volume of each particle type so that the total volume of particles would fill half the tumbler. The rotational speeds of the tube, ω, ranged from 10 to 130 rpm in 10 rpm intervals and were chosen so that the flowing layer was in the continuous cascading flow regime, characterized by a nearly flat free surface, at lower speeds but shifted to the cataracting regime, an "*S*"-shaped flowing layer, at higher rotational speeds [20–23]. These speeds correspond to Froude numbers, $\mathrm{Fr}=\omega^2R/g$, of $3.55\times10^{-3}\leq\mathrm{Fr}\leq0.6$, where R is the radius of the tube and g is the acceleration due to gravity.

A digital camera was synchronized with the stepper motor driving the tumbler to acquire images of the bed of particles. Space-time plots were created by stacking single pixel thick lines of the average intensity over 600 tumbler rotations to track the evolution of band formation. A thresholding algorithm was used to enhance clarity. A phase diagram of space-time plots is shown in Fig. 1.

III. GRANULAR PHASE DIAGRAM

A binary chemical system can undergo phase transitions depending on the free energy of the system and the concentration of the two species. Traditional temperature-composition phase diagrams can be divided into a miscible region and an immiscible region. The miscible region is a single phase in stable equilibrium. The immiscible region is more complicated. If the system falls into metastable equilibrium, concentration fluctuations occur at small localized regions for either low or high fractions of either species. The phase transition is nucleation. At moderate relative concentrations, the system is in unstable equilibrium. Concentration fluctuations occur throughout the entire system as it under-

*jm-ottino@northwestern.edu

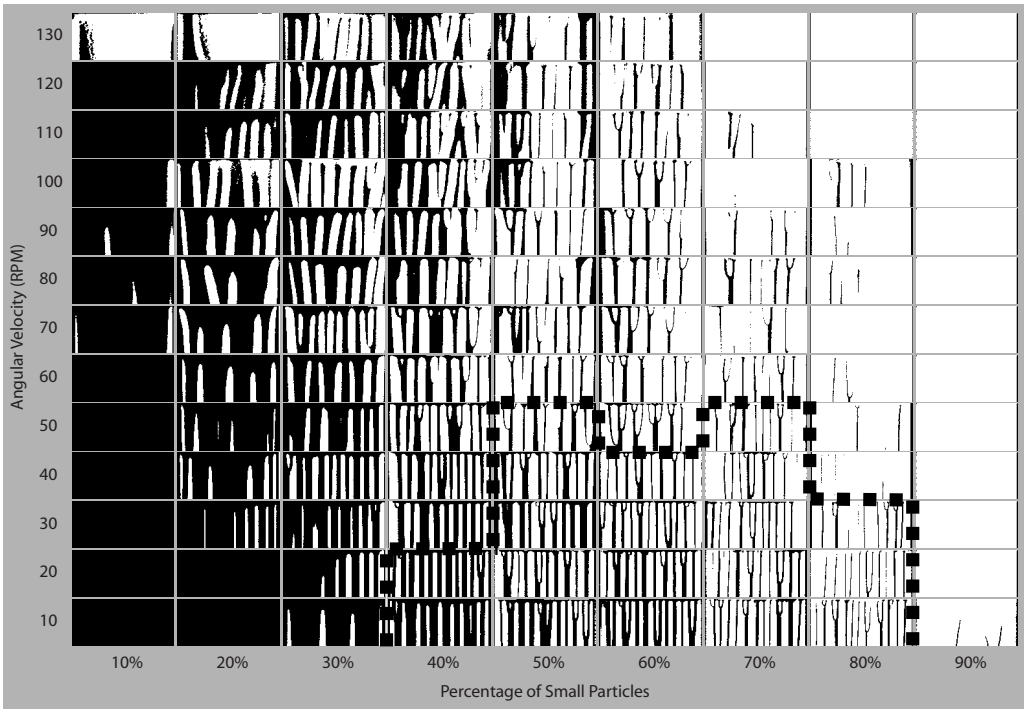

FIG. 1. The matrix of space-time portraits for the liquid granular system shows band formation and evolution as a function of small-particle percentage and angular velocity for 600 tumbler revolutions. In each cell, time progresses from top to bottom. White regions correspond to small particles; dark regions correspond to large particles. The granular nucleation region occurs for small-particle percentages of 20%–40%, 80%, and 90%. The granular spinodal region, bounded approximately by the dotted line, occurs for lower angular velocities in small-particle percentages of 40%–80%.

goes a phase transition known as spinodal decomposition [24,25].

While there is no direct relation between the angular velocity of the tumbler and granular temperature, the granular temperature would be expected to increase with increased angular velocity and therefore plays a similar role as temperature [3]. Based on this simple assumption, there is an analogy between the temperature-composition phase diagram of a binary chemical system and the angular velocity-composition phase diagram for a binary granular system, the matrix of space-time plots in Fig. 1. This analogy can be utilized to categorize a granular system as a granular nucleation region, a granular spinodal region, or a miscible region.

Consider first the miscible region corresponding to a single phase in stable equilibrium. In Fig. 1, the large (dark) particles fill the entire space-time plot in each cell of the matrix at low small-particle fractions (10%), as would be expected, with a few exceptions. At large small-particle concentrations (90%), small particles dominate.

Phase separation analogous to spinodal decomposition occurs for systems at moderate small-particle concentrations. Alternating small and large particle bands form along the length of the tumbler for small-particle concentrations of 40% to 80% for low angular velocities, as shown in Fig. 1. Figure 2 demonstrates four characteristics of the space-time plots that define the spinodal decomposition region within the dotted lines in Fig. 1. First, bands form quickly, on the order of 50 tumbler revolutions, along the entire length of the tumbler. Second, the average wavelength is approximately equal to the tumbler diameter [8,10,17]. Third, the percent surface area [17] of small particles reaches equilibrium within 100 rotations and remains constant [Fig. 2(b)]. And fourth, after reaching a maximum, bands merge and the pattern coarsens, much like spinodal decomposition in a binary chemical system, so that the number of bands decreases logarithmically in a step-wise fashion when the number of revolutions exceeds 40 [9,17] [Fig. 2(c)].

A region corresponding to phase separation which appears like nucleation occurs for granular systems in rotating tumblers at low or high small-particle fractions, as shown in Fig. 1. At low small-particle fractions, 20%–30%, few *small*-particle bands form, less than L/D, and those that form do not merge for almost all angular velocities. At small-particle fractions of 50%–80% at higher angular velocities ($>$60 rpm) and small-particle fraction of 90% at 10 rpm, few *large*-particle bands form along the length of tumbler. Typical space-time plots of nucleation of small- and large-particle bands are shown in Figs. 3(a) and 3(b), respectively. A characteristic of granular nucleation is that it takes much longer for a band to appear at the surface than it does for spinodal band formation, anywhere from 200 to 300 revolutions. Bands often appear near the end walls first and there is slow change in the percent of surface area as a function of tumbler revolutions [Fig. 3(c)]. The number of bands increases slowly in time and bands rarely merge [Fig. 3(d)]. Unlike the situation akin to spinodal decomposition, the band structure is not periodic.

Clearly, axial segregation dynamics depends on the relative particle concentration and the angular velocity of the tumbler. Depending on the parameters of the system, either

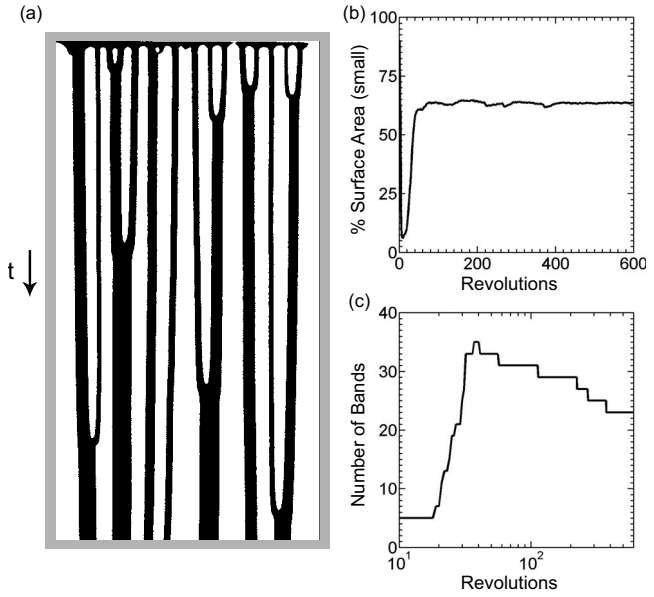

FIG. 2. (a) Space-time plot for a granular mixture with moderate small-particle fraction (2500 rotations, c_s=60% at 10 rpm) typical of those bounded by the dotted line for low angular velocities with small-particle percentages of 40%–80%. (b) The percent surface area of small particles rises sharply and remains constant. (c) The number of bands reaches a maximum and then decreases logarithmically.

no bands appear (such as the miscible region), some bands appear and grow slowly in time with no merging (such as nucleation), or bands appear along the entire length of the tumbler and the segregation pattern coarsens at a logarithmic rate (such as spinodal decomposition). However, it is also evident that the granular phase diagram is much more complicated than for a binary chemical system in that there are

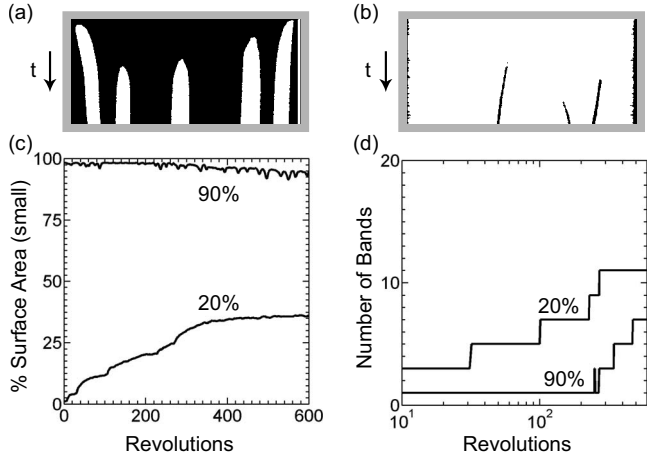

FIG. 3. Typical space-time plot (600 rotations) for a granular mixture in the granular nucleation region. (a) For low small-particle fractions (c_s=20% at 70 rpm), there is nucleation of small-particle bands. (b) For high small-particle fractions (c_s=90% at 10 rpm), there is nucleation of large-particle bands. (c) The percent surface area of small or large particle bands changes slowly in time. (d) The total number of bands increases slowly in time and no merging occurs.

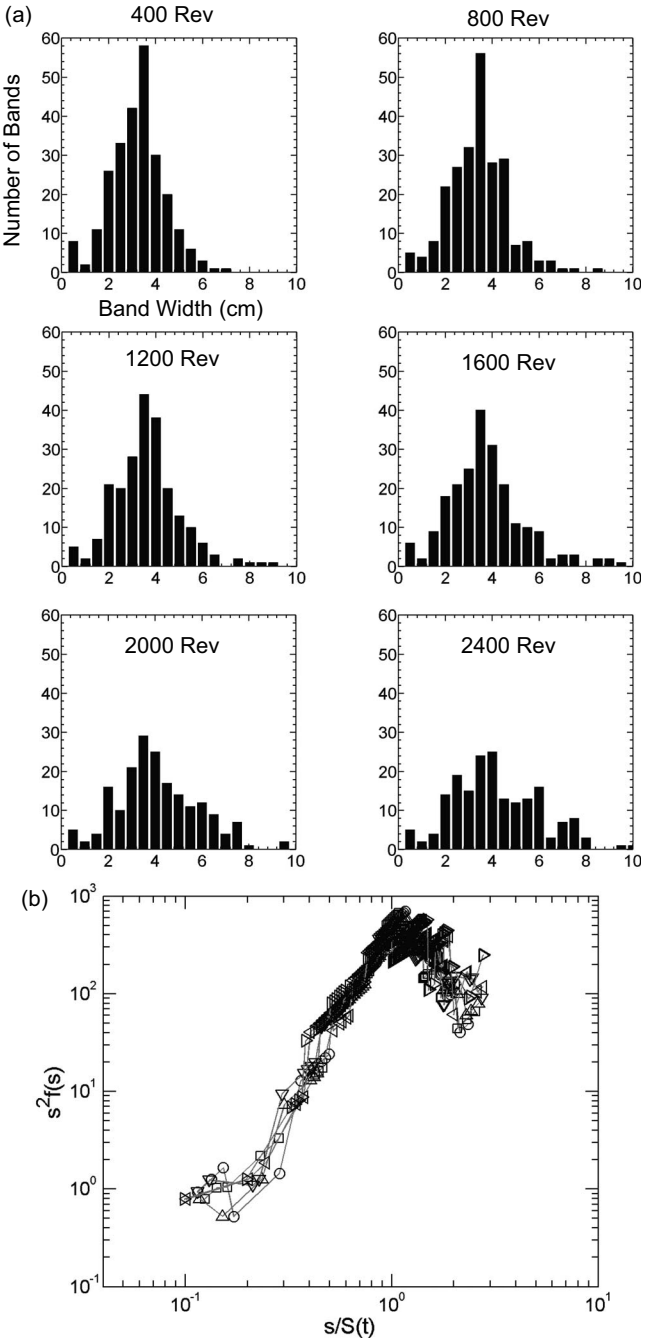

FIG. 4. Example of granular dynamic scaling that applies to any space-time plot bounded by the dotted line in Fig. 1. (a) Histograms of band thickness s at every 400 revolutions. (b) The six curves for the scaling anzatz, $s^2f(s)=s/S(t)$, corresponding to 400 (○), 800 (□), 1200 (△), 1600 (▽), 2000 (◁), and 2400 (▷) revolutions collapse for ten different experiments under the same conditions of c_s=60% at 10 rpm over a duration of 2500 revolutions.

some regions of the phase diagram that do not fit any of the three categories. An example is the unexpected sharp transition from all black at 120 rpm to almost all white at 130 rpm for a small-particle concentration of c_s=10%, the top left corner of Fig. 1. Clearly, interesting phenomena occur at high angular velocities that deserve further investigation.

IV. GRANULAR DYNAMIC SCALING

Scaling arguments are useful to determine if properties of a system are independent of dynamical details. Scaling laws have been previously used to describe the dynamics of a lamellae system in chaotic mixing of fluids, critical phenomena, and aggregation processes [18,19,26,27]. These structures dynamically evolve toward a universal striation thickness distribution, $f(s)$, regardless of initial conditions [18,19]. A similar scaling approach can be used to analyze axial banding systems that undergo logarithmic coarsening.

Consider a system with a distribution, $f(s,t)$, of bands of thickness s. We postulate, $s^{\theta}f(s,t)=g(s/S(t))$, where $g(y)$ is the scaling solution, $y=s/S(t)$ is the scaling argument, and $S(t)$ is the mean band thickness [18,19]. If a band merges and grows, it does so as a neighboring band shrinks. Since the percent surface area of the system remains constant [Fig. 2(b)], the area, $A=\int_0^{\infty}sf(s,t)ds=\int_0^{\infty}s^{1-\theta}g(y)ds=[S(t)]^{2-\theta}\int_0^{\infty}y^{1-\theta}g(y)dy$, is also constant. Since the last integral is independent of time, it then follows that $\theta=2$.

The dynamic scaling analysis is as follows. Since the number of bands in a granular system is small, ten independent space-time plots such as Fig. 2(a) for the same initial conditions are placed side by side, equivalent to a tumbler 10 times its actual length. The band widths of the composite plot provide the mean band thickness, $S(t)$, and histogram of the width distribution, $f(s,t)$, for several times [Fig. 4(a)]. The initial band thickness distribution in Fig. 4(a) is sharply peaked at a band width of about 3 cm, or approximately $D/2$, since the initial system wavelength is on the order of the tumbler diameter. As bands merge, the number of wide bands increases; wide bands grow at the expense of neighboring narrow bands. These values are plotted according to the scaling relation, $s^2f(s)=g[s/S(t)]$, in Fig. 4(b). Regardless of the band thickness distribution and the overall number of bands in the system at different times, the curves for 400–2400 revolutions collapse [Fig. 4(b)]. Similar results occur for all concentrations within the granular spinodal boundary in Fig. 1.

V. CONCLUSIONS

The analogy to phase transitions similar to nucleation and spinodal decomposition as well as a dynamic scaling relation that suggests universality of band thickness distribution provides insight into the axial segregation of binary mixtures in horizontal rotating tumblers. However, there are still issues concerning the onset of axial segregation and the physical origin of the apparent "negative diffusivity" used in phenomenological models for granular systems connected with spinodal decomposition [2,16,28]. Experimental or computational analysis related to the core of small particles beneath the surface that precedes band formation [3,4,12] could help elucidate the origin of nucleation and spinodal decomposition behavior. Clearly, the phase diagram for granular mixtures is complicated and further exploration is needed.

[1] Y. Oyama, Sci. Pap. Inst. Phys. Chem. Res. (Jpn.) **37**, 17 (1940).
[2] O. Zik, D. Levine, S. G. Lipson, S. Shtrikman, and J. Stavans, Phys. Rev. Lett. **73**, 644 (1994).
[3] K. M. Hill, A. Caprihan, and J. Kakalios, Phys. Rev. Lett. **78**, 50 (1997).
[4] T. Arndt, T. Siegmann-Hegerfeld, S. J. Fiedor, J. M. Ottino, and R. M. Lueptow, Phys. Rev. E **71**, 011306 (2005).
[5] A. Alexander, F. J. Muzzio, and T. Shinbrot, Granular Matter **5**, 171 (2004).
[6] H. P. Kuo, Y. C. Hsiao, and P. Y. Shih, Powder Technol. **166**, 161 (2006).
[7] H. P. Kuo, R. C. Hsu, and Y. C. Hsiao, Powder Technol. **153**, 196 (2005).
[8] C. R. J. Charles, Z. S. Khan, and S. W. Morris, Granular Matter **8**, 1 (2006).
[9] S. J. Fiedor and J. M. Ottino, Phys. Rev. Lett. **91**, 244301 (2003).
[10] S. J. Fiedor, P. Umbanhowar, and J. M. Ottino, Phys. Rev. E **73**, 041303 (2006).
[11] K. M. Hill and J. Kakalios, Phys. Rev. E **52**, 4393 (1995).
[12] N. Jain, D. V. Khakhar, R. M. Lueptow, and J. M. Ottino, Phys. Rev. Lett. **86**, 3771 (2001).
[13] T. Finger and R. Stannarius, Phys. Rev. E **75**, 031308 (2007).
[14] K. M. Hill and J. Kakalios, Phys. Rev. E **49**, R3610 (1994).
[15] S. J. Fiedor, P. Umbanhowar, and J. M. Ottino, Phys. Rev. E **76**, 041303 (2007).
[16] K. Choo, T. C. A. Molteno, and S. W. Morris, Phys. Rev. Lett. **79**, 2975 (1997).
[17] G. Juarez, J. M. Ottino, and R. M. Lueptow, Phys. Rev. E **78**, 031306 (2008).
[18] F. J. Muzzio and J. M. Ottino, Phys. Rev. Lett. **63**, 47 (1989).
[19] F. J. Muzzio and J. M. Ottino, Phys. Rev. A **40**, 7182 (1989).
[20] J. M. Ottino and D. V. Khakhar, Annu. Rev. Fluid Mech. **32**, 55 (2000).
[21] J. Rajchenbach, Phys. Rev. Lett. **65**, 2221 (1990).
[22] H. Henein, J. K. Brimacombe, and A. P. Watkinson, Metall. Mater. Trans. B **14**, 191 (1983).
[23] J. Mellmann, Powder Technol. **118**, 251 (2001).
[24] D. V. Ragone, *Thermodynamics of Materials* (Wiley, New York, 1995).
[25] P. Papon, J. Leblond, and P. H. E. Meijer, *The Physics of Phase Transitions, Concepts and Applications* (Springer-Verlag, Berlin, 2006).
[26] P. C. Hohenberg and B. I. Halperin, Rev. Mod. Phys. **49**, 435 (1977).
[27] P. G. J. van Dongen and M. H. Ernst, J. Stat. Phys. **50**, 295 (1988).
[28] I. S. Aranson and L. S. Tsimring, Phys. Rev. Lett. **82**, 4643 (1999).